Performance of Energy Harvesting Cooperative Cognitive Radio Network under Higher order QAM Schemes

Banani Talukdar[1], Deepak Kumar[2], and Wasim Arif[3]

Abstract— **Cognitive radio (CR) with adaptive modulation schemes can resolve the spectrum scarcity problem and fulfill the high data-rate requirement for the deployment of the nextgeneration wireless network. Here, we examine the performance of an energy harvesting cognitive radio network (EH-CRN) based on cooperative prediction-sensing, over Nakagami-m fading channels for higher-order modulation schemes like rectangular quadrature amplitude modulation (RQAM) and hexagonal QAM (HQAM). These schemes provide high data rates with improved power and spectral efficiency. For performance analysis, the exact analytical expressions of energy harvesting, throughput, outage probability, and average symbol error rate (ASER) are derived. The impact of fading severity, threshold data-rate, and constellation size on the system performance is highlighted. The simulation results prove the correctness of the derived exact analytical expressions.**

Clinical relevance— **This establishes the efficacy of adaptive modulation. Higher-order QAM modulation techniques are a potential solution for high data rate transmission with better power and spectrum efficiency**

I. INTRODUCTION

Data traffic has soared due to the rapid evolution of wireless applications and the enormous growth of mobile users [1]. Therefore, more radio spectrum is required to enable high speed data networks [2]. Effective spectrum management policies are required for communication networks to work successfully [3]. As a result, cognitive radio (CR) technology posed as a viable solution to address the spectrum shortage in wireless communication. In addition, an energy-harvesting technique is envisioned as propitious solution to overcome the energy constraint for the wireless communication systems [4], [5], [6], [7]. In [8], [9], [10], [11], EH-enabled CRN is extensively investigated, improving both spectrum and energy efficiency.

The performance of CR can be analyzed at the node, network, and application levels using a variety of performance measures. One typical performance indicator considered for CR users is the transmission rate. However, the error rate is also an important performance metric that estimates the reliability of CR communications. Consequently, a number of recent studies [12], [13] include error rate in CR analysis. The improvement of network quality is dependent on a variety of factors, and one of the key factors to improve network performance is modulation techniques. Most CR networks (CRNs) employ binary phase shift keying (BPSK) as the fundamental modulation technique. However, in LTE-Advanced standards and future technologies, quadrature amplitude modulation (QAM) is the ideal modulation technique to deliver high data rates due to its excellent power and bandwidth efficiency.

In the next generation wireless communication networks, the transmission of high data rates while maintaining power and spectrum efficiency are major concerns. To overcome both the concerns, an adaptive modulation technique can turns out to be a practical solution [14], [15]. Higher-order QAM modulation techniques are a potential solution for high data rate transmission with better power and spectrum efficiency. The family of QAM includes several significant QAM constellations namely, square QAM (SQAM), rectangular QAM (RQAM), and hexagonal QAM (HQAM)[16]. RQAM is a flexible and general order modulation technique. It consists of SQAM, BPSK, quadrature phase-shift keying (QPSK), and others as special cases [17], and it is widely used in telecommunication systems, microwave etc.

HQAM has highly compact 2D constellations that provide low peak-to-average power. Due to its supremacy over the other constellations, HQAM is preferred for a wide range of applications namely multiple-antenna systems, advanced channel coding etc. The performance of QAM techniques employed in various communication systems over various fading channels has been studied and reported on by researchers in a number of papers [18], [19], [20], [21], [22]. Under the Nakagami-m fading channel, [19], calculates the average symbol error rate (ASER) expression for RQAM, QPSK, and differentially encoded QPSK. In [20], the authors constructed the exact ASER expressions of RQAM and cross QAM in an amplify and forward (AF) multiple relay network over Rayleigh fading channels. The authors investigate the performance of a SC receiver using HQAM and RQAM over $k-\mu$ fading channels [21]. [22]evaluated a novel analytical symbol error probability (SEP) for HQAM.

To effectively utilize the scarce spectrum with optimum power, the QAM schemes particularly RQAM and HQAM are adopted in this work for a cooperative CRN. We analyze the performance of a cooperative prediction-sensing based EHCRN under a Nakagami-m fading channel and use higherorder QAM constellations for high data rate, spectrally efficient, and low ASER communication. To acquire better system performance, the exact analytical expression of

*This work was not supported by any organization

[1] Banani T. Researcher is with the Department of Electronics and Communication Engineering, National Institute of Technology Silchar, Silchar, India talukdarbanani.smit@gmail.com

[2] Deepak K.. Researcher is with the Department of Electrical Engineering, Indian Institute of Technology Indore, Indore, India phd1901102017@iiti.ac.in

[3] Wasim A. is with Faculty of Electronics and Communication Engineering, National Institute of Technology Silchar, Silchar, India arif@ece.nits.ac.in

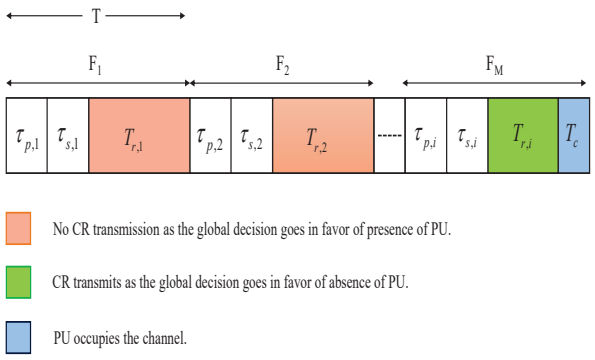

Fig. 1. PU detection frame.

ASER for RQAM and HQAM constellations is determined. The ASER performance for several QAM constellations is examined in order to validate the supremacy of RQAM and HQAM. Lastly, the mathematical modelling of the system is established by using Monte Carlo simulation.

The Remaining paper is structured as: Section II provides the system model. Performance analysis is reported in Section III. Numerical findings are discussed in Section IV. Conclusions are put forward in Section V.

II. SYSTEM MODEL

We assume a cooperative EH-CRN comprised of a PU transmitter, a fusion center (FC) and a group of CR users. Each CR user consists of an energy harvester and an energy splitting device. The harvester is capable of harvesting energy out of RF signal emanating from the PU as well as non-RF signals. This harvested energy is saved in an energy buffer having infinite capacity such as a supercapacitor. The CR user predicts and senses for the presence of PU in a time-slotted model. The CR users freely predict for the presence of PU in the channel and forward the prediction results to the FC to get final information about the existence of PU. The CR users next cooperatively sense the channel for the existence of PU and forward the sensing information to the FC to yield the cooperative decision. In either case, the FC employs a hard combining rule i.e., OR rule to determine the ultimate decision pertaining to the presence of PU. Lastly, the FC communicates the final decision as a set of four level-quantized decision which can be either of $00, 10, 01, 11$ where the initial bit is the final prediction decision and the subsequent bit is the final sensing decision.

All the frames of the CR user are made up of prediction, sensing and transmission periods and are expressed as τ_p, τ_s, and T_r, respectively, as shown in Fig. 1. In addition, the CR user is unfamiliar with the PU signal, which is arbitrary. It is to be noted that there is likelihood that the PU may re-claim spectrum access amidst ongoing CR transmissions.

A. PU Activity model

The two distinct states of the PU i.e., busy and idle states are modeled as a two state Markov model. Both states have an exponential time distribution with mean b and a for the two hypotheses $\mathscr{H}_0$ and $\mathscr{H}_1$. $\mathscr{H}_0$ stands for absence of PU and the alternate hypotheses $\mathscr{H}_1$ stands for PU occupancy. The expression of probability density functions (PDFs) of both the states are

$$P_B(t) = \frac{1}{b} e^{\frac{-t}{b}} \; ; \; P_I(t) = \frac{1}{a} e^{\frac{-t}{a}}, \tag{1}$$

respectively. Here,$P(\cdot)$ gives the probability. Given that the PU regains channel access, and as such, there exist some probable hypotheses corresponding to the PU channel possession state of the specified channel [23].

B. Channel Prediction

The CR users in the cooperative network predicts about the channel occupation of PU based on the prior information about the PU activity. The overall prediction $\hat{X}_P$ is a function of the individual prediction outcomes $\hat{x}_{Pi}$. Consequently, the overall prediction is formulated as,

$$\hat{X}_P = f(\hat{x}_{P1}, \hat{x}_{P2}, \hat{x}_{P3}, \cdots \hat{x}_{PN}) \tag{2}$$

Here, $f(\cdot)$ is the fusion rule.

C. Channel Sensing

After sampling the received signal at f_s Hz, the number of samples, $N_s = \tau_s f_s$ is calculated. The received signal $Y_{CR_i}(n)$ at the CR user can be described as

$$Y_{CR_i}(n) = \begin{cases} hs(n) + u(n) & , \text{for } \mathscr{H}_1 \\ u(n) & , \text{for } \mathscr{H}_0 \end{cases} \tag{3}$$

We assume the following: a) $u(n)$ is the i.i.d AWGN noise signal having mean and variance as 0 and ${\sigma_u}^2$, respectively. Also, h represents the channel-fading coefficient;b) $s(n)$ indicates the primary user signal having mean zero and variance ${\sigma_s}^2$. The decision statistics of the ED can be given by

$$T_{CR_i} = \frac{1}{N_s} \sum_{n=1}^{N_s} |Y_{CR_i}(n)^2|. \tag{4}$$

The decision statistic approaches a Gaussian distribution for a bigger number of samples. Each of the CR users compare their decision statistics with a fixed threshold value, λ_{CR}. Consequently, the sensing probabilities at the i-th CR in case of an ideal ED can be calculated as given in [23].

We use a Nakagami-m statistical fading model to demonstrate an easy and precise ASER analysis of RQAM and HQAM. The envelope of the faded signal in a Nakagami-m fading channel has a PDF given as

$$f_\gamma(\gamma) = \frac{1}{\Gamma(m)} \left(\frac{m}{\bar{\gamma}}\right)^m \gamma^{m-1} \exp\left(-\frac{m}{\bar{\gamma}}\gamma\right), \gamma \geq 0 \tag{5}$$

where m refers to the fading severity parameter. The average probability of detection, $\tilde{P}_{d,Nak}$, is given as

$$\tilde{P}_{d,Nak} = A_1 + \beta^m e^{-\frac{\lambda}{2\sigma^2}} \times \sum_{i=0}^{N/2-2} \frac{\left(-\frac{\lambda}{2\sigma^2}\right)^i}{i!} \times {}_1F_1\left(m; i+1; \frac{-\lambda(1-\beta)}{2\sigma^2}\right). \tag{6}$$

Here, $A_1 = e^{-\frac{\lambda\beta}{2m\sigma^2}}\left[\beta^{m-1}L_{m-1}\left(\frac{-\lambda(1-\beta)}{2\sigma^2}\right) + (1-\beta)\sum_{i=0}^{m-2}\beta^i L_i\left(\frac{-\lambda(1-\beta)}{2\sigma^2}\right)\right]$, $\beta = \frac{2m\sigma^2}{(2m\sigma^2+\alpha\bar{\gamma})}$, and ${}_1F_1(.;.;.)$ indicates the confluent hypergeometric function [24]. The false alarm probability does not change because it does not include any terms related to the fading channel parameters. The final channel sensing decisions are calculated as given in [23].

D. Hard Combined Decision

The choice of data transmission and the form of energy harvesting source is determined by the CR; once the outcomes of prediction and sensing mechanisms are obtained. Both these outcomes are coupled to form the hard combined decision. Please note that both the prediction and sensing mechanisms are mutually independent.

III. PERFORMANCE ANALYSIS

A. Energy Harvesting

The proposed model is incorporated with energy harvesting, allowing a CR user to collect energy from RF and non-RF sources. During prediction-sensing time, the CR user leaves both the harvesters on, as the CR user is unaware of the presence of PU. Accordingly, there arises a necessity of determining the probability of when the PU remains busy during the prediction-sensing time. This probability is given

$$P_{ac} = \int_0^{\tau_p+\tau_s} P_B(t)dt. \tag{7}$$

The energy harvested can be calculated by [23]

$$\begin{aligned} E_H =& M[(1-P_{ac})E_{nrf} + P_{ac}E_{rf}(\tau_p+\tau_s) + E_1 + E_2] \\ &+ X^{M-1}[P(\mathscr{H}_0)P_f(T_r-T_c)E_{nrf} + T_cE_{rf}]. \end{aligned} \tag{8}$$

where, E1, E2 are expressed as

$$E_1 = P(\mathscr{H}_1)P_d(1-P_{dis})T_rE_{rf}, \tag{9}$$

and

$$E_2 = T_rE_{nrf}[P(\mathscr{H}_1)P_m + P(\mathscr{H}_1)P_{AM1} + P(\mathscr{H}_0)P_{AM2}], \tag{10}$$

respectively. For multiple detection frames, a CR reports the channel occupation of PU for $(M-1)$ frames and initiates transmission in the M^{th} frame when the PU vacates the channel.

B. Throughput

We observe successful transmissions only when the hard combined decision declares $P(\hat{X}_P = \mathscr{H}_0, X_S = \mathscr{H}_0|\mathscr{H}_0)$. Then, the secondary network throughput is given

$$\begin{aligned} R_{0M} =& \left[\frac{T-\tau_p-\tau_s-T_c}{T}\right]P(\mathscr{H}_0)[P(\mathscr{H}_1)(P_d+P_{AM1}) \\ &+ P(\mathscr{H}_0)(P_f+P_{AM2})]^{(M-1)}P_{nf}C_0. \end{aligned} \tag{11}$$

C. Outage Probability

The outage probability is denoted P_{out} and is described as the link failure probability where the instantaneous SNR, γ_{inst} lies below a preset threshold SNR, γ_{th}. Mathematically, the outage probability is defined as [25]

$$P_{out} = \int_0^{\gamma_{th}} f_\gamma(\gamma)d\gamma \tag{12}$$

where, $f_\gamma(\gamma)$ characterizes the PDF of the fading channel. The threshold SNR is determined by $\gamma_{th} = 2^R - 1$ where R denotes the desired transmission rate. Utilizing (5), the OP for a Nakagami-m faded channel is calculated as

$$P_{out} = \frac{1}{\Gamma(m)}\gamma\left(m, \frac{m\sigma^2\gamma_{th}}{\bar{\gamma}P_s}\right) \tag{13}$$

Here, $\Gamma(\cdot)$ and $\gamma(\cdot,\cdot)$ portrays the complete and incomplete Gamma functions.

D. Average Symbol Error Rate (ASER)

The average symbol error rate (ASER) is another key performance criterion and is perhaps the most critical parameter to evaluate. A generalized expression for ASER based on the CDF of a digital modulation scheme is expressed as

$$P_s(e) = -\int_0^\infty P_s'(e|\gamma)P_{out}(\gamma)d\gamma \tag{14}$$

For the received signal SNR, $P_s'(e|\gamma)$ is the first-order derivative of the conditional ASER $P_s(e|\gamma)$. For the ASER analysis to be more compliant the outage probability is considered for analysis.

1) Rectangular QAM (RQAM): The analytical formula of ASER for M-ary RQAM modulation technique for Nakagami-m fading channels is given in (15), where $p = 1-\left(\frac{1}{M_I}\right), q = 1-\left(\frac{1}{M_Q}\right), a = \sqrt{\frac{6}{(M_I^2-1)(M_Q^2-1)\lambda^2}}$, $b = \lambda a$, $\Psi_1 = \sum_{r_1=0}^{\infty}\frac{(1)r_1}{r_1!\frac{3}{2}r_1}\left(\frac{a^2}{2}\right)^{r_1}$, $\Psi_2 = \sum_{r_2=0}^{\infty}\frac{(1)r_2}{r_2!\frac{3}{2}r_2}\left(\frac{b^2}{2}\right)^{r_2}$, and $\Psi_3 = \sum_{n=0}^{m-1}\frac{1}{n!}\left(\frac{m\sigma^2}{\Omega P_s}\right)$. M_I is the in phase constellation points and M_Q is the quadrature phase constellation points.

2) Hexagonal QAM (HQAM): The analytical formula of ASER for M-ary HQAM modulation technique is given in (16), where α, τ, and τ_c are constant terms, provided their values are adjusted so as to obtain the required HQAM constellation [22].

IV. RESULTS AND DISCUSSION

In this section, the derived mathematical expressions for the different performance metrics are numerically evaluated and the plots are obtained using MATLAB and Mathematica software. The simulation results substantiate the exactness of the mathematical modelling of the system.

The harvested energy in relation to the sensing channel SNR for various fading severity parameters is shown in Fig. 2. In a Nakagami-m channel, m characterizes the fading severity parameter. We observe that the harvested energy increases as the fading severity parameter rises. A larger

$$P_s(e) = -p(q-1) - (p-1)q + \frac{abpq}{\pi}\left[\Psi_1(r_1!)\left(\frac{a^2+b^2}{2}\right)^{-r_1-1} + \Psi_2(r_2!)\left(\frac{a^2+b^2}{2}\right)^{-r_2-1}\right] + \Psi_3\frac{ap(q-1)}{\sqrt{2\pi}} \times \frac{\Gamma(n+\frac{1}{2})}{\left(\frac{a^2}{2}+\frac{m\sigma^2}{\bar{\gamma}P_s}\right)^{n+\frac{1}{2}}} + \Psi_3\frac{bq(p-1)}{\sqrt{2\pi}}\frac{\Gamma(n+\frac{1}{2})}{\left(\frac{b^2}{2}+\frac{m\sigma^2}{\bar{\gamma}P_s}\right)^{n+\frac{1}{2}}} - \frac{abpq}{\pi}\Psi_3\left[\Psi_1\frac{\Gamma(n+r_1+1)}{\left(\frac{a^2+b^2}{2}+\frac{m\sigma^2}{\bar{\gamma}P_s}\right)^{(n+r_1+1)}} + \Psi_2\frac{\Gamma(n+r_2+1)}{\left(\frac{a^2+b^2}{2}+\frac{m\sigma^2}{\bar{\gamma}P_s}\right)^{(n+r_2+1)}}\right] \tag{15}$$

$$P_s(e) = \frac{\tau}{2} - \frac{2}{3}\tau_c - \frac{2\tau_c\alpha}{9\pi}\Psi_1 r_1!\left(\frac{2\alpha}{3}\right)^{-r_1-1} + \frac{\tau_c\alpha}{2\sqrt{3}\pi}\Psi_2 r_2!\left(\frac{2\alpha}{3}\right)^{-r_2-1} + \frac{\tau_c\alpha}{2\sqrt{3}\pi}\Psi_3 r_3!\left(\frac{2\alpha}{3}\right)^{-r_3-1} + \frac{1}{2}\sqrt{\frac{\alpha}{2\pi}} \times (\tau_c-\tau)\Psi_4\frac{\Gamma(\frac{n+1}{2})}{\left(\frac{\alpha}{2}+\frac{m\sigma^2}{\bar{\gamma}}\right)^{\frac{n+1}{2}}} - \frac{\tau_c}{3}\frac{\alpha}{3\pi}\Psi_4\frac{\Gamma(\frac{n+1}{2})}{\left(\frac{\alpha}{2}+\frac{m\sigma^2}{\bar{\gamma}}\right)^{\frac{n+1}{2}}} + \frac{\tau_c}{2}\sqrt{\frac{\alpha}{6\pi}}\Psi_4\frac{\Gamma(\frac{n+1}{2})}{\left(\frac{\alpha}{6}+\frac{m\sigma^2}{\bar{\gamma}P_s}\right)^{\frac{n+1}{2}}} + \frac{2\tau_c\alpha}{9\pi} \times \Psi_1\Psi_4\frac{\Gamma(n+r_1+1)}{\left(\frac{2\alpha}{3}+\frac{m\sigma^2}{\bar{\gamma}P_s}\right)^{(n+r_1+1)}} - \frac{\tau_c\alpha}{2\sqrt{3}\pi}\Psi_2\Psi_4\frac{\Gamma(n+r_2+1)}{\left(\frac{2\alpha}{3}+\frac{m\sigma^2}{\bar{\gamma}P_s}\right)^{(n+r_2+1)}} - \frac{\tau_c\alpha}{2\sqrt{3}\pi}\Psi_3\Psi_4\frac{\Gamma(n+r_3+1)}{\left(\frac{2\alpha}{3}+\frac{m\sigma^2}{\bar{\gamma}P_s}\right)^{(n+r_3+1)}} \tag{16}$$

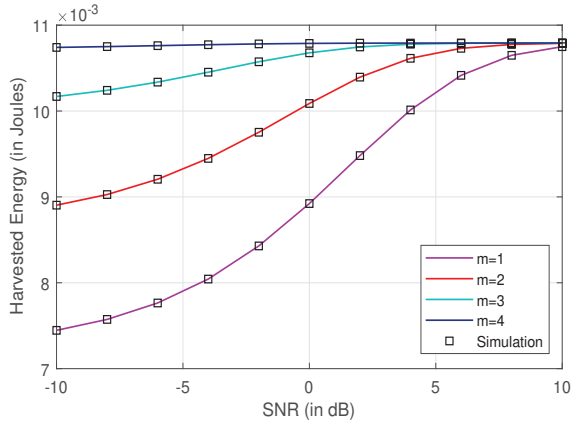

Fig. 2. Harvested energy vs SNR for $m = 1, 2, 3$ and 4.

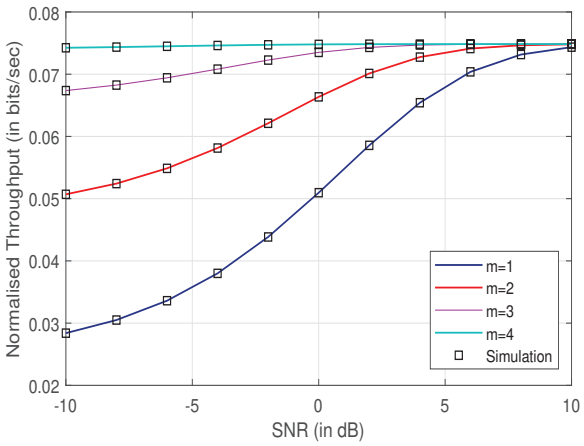

Fig. 3. Normalized throughput for different SNR.

value of m indicates a greater signal strength and confines the signal variations within an admissible limit. When $m = 1$, the Nakagami-m fading is analogous to a Rayleigh fading channel. In this case, $m = 1$ indicates the most severe channel fading.

The variation of the normalized throughput with the sensing channel SNR is illustrated in Fig. 3. The impact of fading severity parameter on the normalized throughput is shown. The normalized throughput begins to rise as the fading severity parameter increases. This is because larger the value of m, less severe is the fading scenario. Since, $m = 1$ indicates the most severe channel fading condition (Rayleigh fading), therefore, the system throughput deteriorates when $m = 1$.

The OP versus SNR for various data rate parameters is shown in Fig.4. It is apparent that the OP drops as the SNR increases. The OP also depends on the data rate parameter such that a higher data rate results in poor outage behavior. For various fading severity values ($m = 1, m = 2$ and $m = 3$) the OP is indicated. The OP falls as the fading depth parameter increases. A rising fading severity parameter implies less severe fading condition and hence, the probability of a CR node moving into outage decreases. The simulations are performed and it can be seen that the simulation and analytical results match well with each other.

The OP as a function of the normalized distance for various fading severity parameters is shown in Fig. 5. The OP is evaluated for different SNR levels and fading severity parameters. The OP increases as the normalized distance

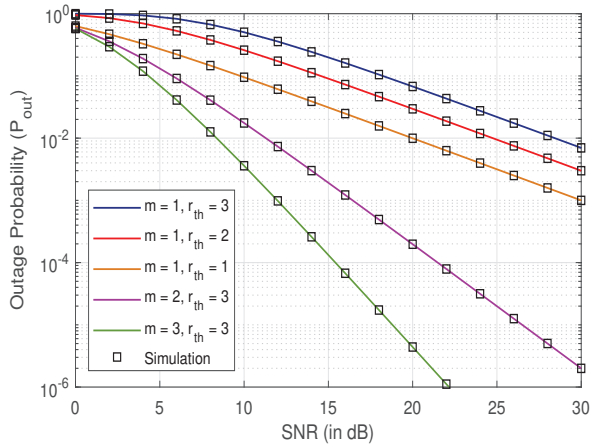

Fig. 4. OP vs SNR for various data rate parameter.

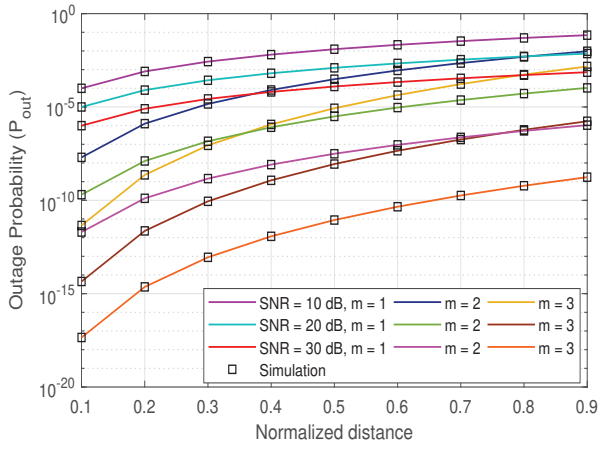

Fig. 5. OP vs normalized distance for various fading severity parameter.

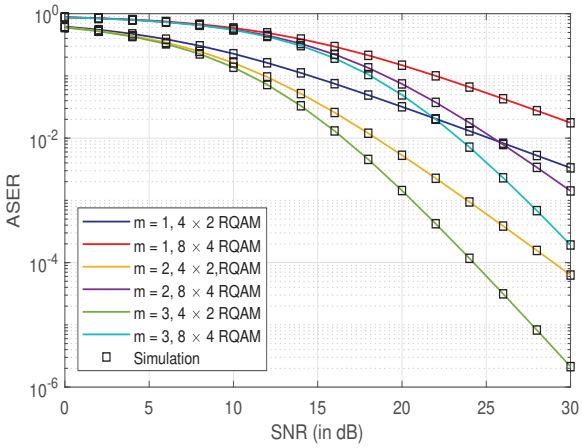

Fig. 6. ASER for Rectangular QAM.

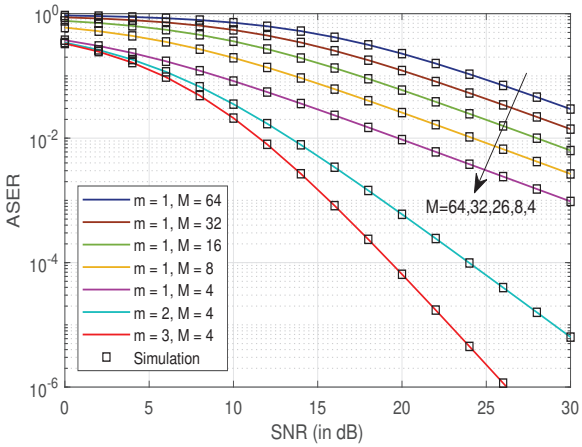

Fig. 7. ASER for Hexagonal QAM.

between the base station and the CR nodes increases. As the normalized distance increases the signal strength decreases and hence, the prospects of a CR node to move into outage is more. The outage probability decreases as the SNR as well as the fading severity parameter increases which is desirable.

Fig. 6 illustrates the ASER performance for 4×2 RQAM and 8×4 RQAM technique for the generalized Nakagami-m fading channels. It is observed that the ASER performance of the considered network improves with the severity parameter m. Further, it is observed that the ASER performance degrades with increase in order of the modulation scheme. To achieve an ASER of 10^{-2} for $m=3$, approximately 7.2 dB gain is achieved when 4×2 RQAM is compared with 8×4 RQAM.

The ASER vs SNR curve for HQAM is shown in Fig. 7. The HQAM modulation technique for various modulation orders M and fading severity parameter ($m=1,2,3$) is shown. The ASER performance degrades with the increases in the modulation order. However, the ASER performance improves with the fading severity parameter m. To attain an ASER of 10^{-2}, approximately 6.5 dB and 8 dB gains are achieved when m increases from 1 to 2 and 1 to 3, respectively.

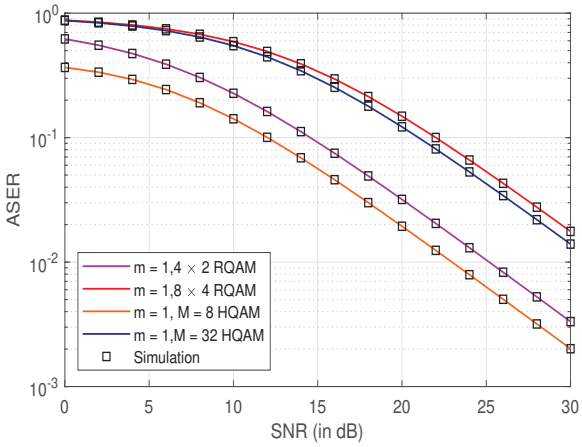

Fig. 8. ASER comparison for RQAM and HQAM.

4 HQAM for a fading severity of $m = 3$, has the least ASER which is desirable. The extent of fading diminishes as the fading severity factor increases, and subsequently the ASER reduces. Fig. 8 analogizes the numerical and simulation results of RQAM and HQAM. HQAM outperforms RQAM by a wide margin. This is because HQAM has a highly dense 2D packing structure compared to the RQAM, which provides low peak and average powers. To attain an ASER of 10^{-1}, we achieve roughly about 1.08 dB and 2.54 dB gain when 32 HQAM and 8 HQAM are compared with 8×4 RQAM and 4×2 RQAM, respectively.

V. CONCLUSIONS

This article evaluates the behavior of a prediction-sensing based EH-CRN under the generalized Nakagami- m fading channel for high data rate communications. The system performance is analyzed in terms of the harvested energy, throughput, OP, and ASER for specific network parameters such as fading severity, threshold data rate, and constellation size. The closed-form expressions of OP and ASER for RQAM and HQAM modulation schemes are derived. The OP decreases as the SNR and the fading severity parameter increase, which is desirable. The ASER performance is valid for the different values of fading severity factor. It is found that the HQAM offers better performance in comparison to other QAM techniques under the presented scenario. The result of the Monte Carlo simulation establishes the appropriateness of the analytical modeling of the system. The higher order QAM modulations will enable the development of extremely reliable, versatile, and efficient broadcasting as well as mobile communication networks owing to its high data-rate with excellent spectral efficiency. The considered system model can be practically implemented for the 5G and beyond network systems to improve both spectral as well as energy efficiency.

REFERENCES

[1] R. Pepper, "Cisco visual networking index (VNI) global mobile data traffic forecast update," Technical report, Cisco, Tech. Rep., 2013.

[2] S. K. Agrawal, A. Samant, and S. K. Yadav, "Spectrum sensing in cognitive radio networks and metacognition for dynamic spectrum sharing between radar and communication system: A review," Physical Communication, p. 101673, 2022.

[3] S. Sanyal, R. Bhadauria, and C. Ghosh, "Secure communication in cognitive radio networks," in 2009 4th International Conference on Computers and Devices for Communication (CODEC). IEEE, 2009, pp. 1–4.

[4] D. K. Verma, R. Y. Chang, and F.-T. Chien, "Energy-assisted decodeand-forward for energy harvesting cooperative cognitive networks," IEEE Transactions on Cognitive Communications and Networking, vol. 3, no. 3, pp. 328–342, 2017.

[5] S. Park and D. Hong, "Optimal spectrum access for energy harvesting cognitive radio networks," IEEE Transactions on Wireless Communications, vol. 12, no. 12, pp. 6166–6179, 2013.

[6] B. Talukdar, D. Kumar, and W. Arif, "Analytical modelling and performance evaluation of a prediction based EH-cooperative CRN under erlang distribution," in 2019 IEEE International Conference on Advanced Networks and Telecommunications Systems (ANTS). IEEE, 2019, pp. 1–6.

[7] S. Park and D. Hong, "Achievable throughput of energy harvesting cognitive radio networks," IEEE Transactions on Wireless Communications, vol. 13, no. 2, pp. 1010–1022, 2014.

[8] B. Talukdar, D. Kumar, and W. Arif, "Performance analysis of a prediction-sensing based cooperative energy harvesting CRN over rician fading channels," Wireless Personal Communications, vol. 127, no. 4, pp. 3637–3658, 2022.

[9] J. Yang and S. Ulukus, "Optimal packet scheduling in a multiple access channel with energy harvesting transmitters," Journal of Communications and Networks, vol. 14, no. 2, pp. 140–150, 2012.

[10] B. Talukdar, D. Kumar, S. Hoque, and W. Arif, "Estimation based cyclostationary detection for energy harvesting cooperative cognitive radio network," Telecommunication Systems, pp. 1–18, 2022.

[11] K. Tutuncuoglu and A. Yener, "Optimum transmission policies for battery limited energy harvesting nodes," IEEE Transactions on Wireless Communications, vol. 11, no. 3, pp. 1180–1189, 2012.

[12] D. Xu, Z. Feng, and P. Zhang, "Minimum average ber power allocation for fading channels in cognitive radio networks," in 2011 IEEE Wireless Communications and Networking Conference. IEEE, 2011, pp. 78–83.

[13] L. Li, P. I. Derwin, and M. Pesavento, "Symbol error rate analysis in multiuser underlay cognitive radio systems," in 2011 IEEE 22nd International Symposium on Personal, Indoor and Mobile Radio Communications. IEEE, 2011, pp. 681–684.

[14] D. Kumar, P. K. Singya, and V. Bhatia, "ASER analysis of hybrid receiver based SWIPT two-way relay network," IEEE Trans. Veh. Technol., vol. 70, no. 10, pp. 10 018–10 030, Oct. 2021.

[15] P. K. Singya, P. Shaik, N. Kumar, V. Bhatia, and M.-S. Alouini, "A survey on higher-order qam constellations: Technical challenges, recent advances, and future trends," IEEE Open Journal of the Communications Society, vol. 2, pp. 617–655, 2021.

[16] D. Kumar, P. K. Singya, O. Krejcar, K. Choi, and V. Bhatia, "Performance of IRS-aided FD two-way communication network with imperfect SIC," IEEE Trans. Veh. Technol., 2023.

[17] P. K. Singya, N. Kumar, V. Bhatia, and M.-S. Alouini, "On performance of hexagonal, cross, and rectangular qam for multi-relay systems," IEEE Access, vol. 7, pp. 60 602–60 616, 2019.

[18] P. K. Singya, N. Kumar, V. Bhatia, and F. A. Khan, "Performance analysis of ofdm based 3-hop af relaying network over mixed rician/rayleigh fading channels," AEU-International Journal of Electronics and Communications, vol. 93, pp. 337–347, 2018.

[19] D. Dixit and P. Sahu, "Performance analysis of rectangular qam with sc receiver over nakagami-m fading channels," IEEE communications letters, vol. 18, no. 7, pp. 1262–1265, 2014.

[20] N. Kumar, V. Bhatia, and D. Dixit, "Performance analysis of qam in amplify-and-forward cooperative communication networks over rayleigh fading channels," AEU-International Journal of Electronics and Communications, vol. 72, pp. 86–94, 2017.

[21] D. Dixit, N. Kumar, and A. K. Mandpura, "On the aser performance of sc receiver with rqam and hqam over $k-\mu$ fading," AEU-International Journal of Electronics and Communications, vol. 138, p. 153883, 2021.

[22] L. Rugini, "Symbol error probability of hexagonal qam," IEEE communications letters, vol. 20, no. 8, pp. 1523–1526, 2016.

[23] A. Bhowmick, K. Yadav, S. D. Roy, and S. Kundu, "Throughput of an energy harvesting cognitive radio network based on prediction of primary user," IEEE Transactions on Vehicular Technology, vol. 66, no. 9, pp. 8119–8128, 2017.

[24] I. S. Gradshteyn and I. M. Ryzhik, Table of Integrals, Series, and Products. Academic Press, 2014.

[25] M. K. Simon and M.-S. Alouini, "Digital communications over fading channels (mk simon and ms alouini; 2005)[book review]," IEEE Transactions on Information Theory, vol. 54, no. 7, pp. 3369–3370, 2008.